Single-fiber diffuse optical time-of-flight spectroscopy

Alerstam, Erik; Svensson, Tomas; Andersson-Engels, Stefan; Spinelli, Lorenzo; Contini, Davide; Dalla Mora, Alberto; Tosi, Alberto; Zappa, Franco; Pifferi, Antonio

Published in:
Optics Letters

DOI:
10.1364/OL.37.002877

2012

Single-fiber diffuse optical time-of-flight spectroscopy

Erik Alerstam,[1,*] Tomas Svensson,[1] Stefan Andersson-Engels,[1] Lorenzo Spinelli,[2] Davide Contini,[3] Alberto Dalla Mora,[3] Alberto Tosi,[4] Franco Zappa,[4] and Antonio Pifferi[2,3]

[1]*Department of Physics, Lund University, P.O. Box 118, 221 00 Lund, Sweden*

[2]*Istituto di Fotonica e Nanotecnologie–CNR, Piazza Leonardo da Vinci 32, 20133 Milano, Italy*

[3]*Dipartimento di Fisica, Politecnico di Milano, Piazza Leonardo da Vinci 32, 20133 Milano, Italy*

[4]*Dipartimento di Elettronica e Informazione, Politecnico di Milano, Piazza Leonardo da Vinci 32, 20133 Milano, Italy*

**Corresponding author: erik.alerstam@fysik.lth.se*

Received December 22, 2011; revised April 2, 2012; accepted May 7, 2012;
posted May 29, 2012 (Doc. ID 160099); published July 11, 2012

We demonstrate interstitial diffuse optical time-of-fight spectroscopy based on a single fiber for both light delivery and detection. Detector saturation due to the massive short-time reflection is avoided by ultrafast gating of a single photon avalanche diode. We show that the effects of scattering and absorption are separable and that absorption can be assessed independently of scattering. Measurements on calibrated liquid phantoms and subsequent Monte Carlo–based evaluation illustrate that absorption coefficients can be accurately assessed over a wide range of medically relevant optical properties. Our findings pave the way to simplified and less invasive interstitial *in vivo* spectroscopy.

OCIS codes: 170.6510, 290.5820.

Minimally invasive *in vivo* spectroscopy based on needle-guided optical fibers is an attractive tool for medical applications, from tissue diagnostics in general to characterization of suspect tissue lesions [1–8]. Ensuring that spectroscopic signals are representative of the tissue studied is of major concern, and it is not a simple matter. By utilizing source and detector fibers separated by a few centimeters, one ensures that signals reflect an average of a large tissue volume. The drawback is increased invasiveness and a need of exact control of geometry (positioning), limiting clinical applicability. Using contiguous fibers (or a single fiber) reduces invasiveness and relaxes the need of control over positioning but generally limits the probed volume to a superficial region close to the fiber tip. The spectroscopic signal may thus be dominated by inhomogeneities and changes caused by the probe, i.e., bleeding. However, in previous theoretical studies [9,10], it was shown that the mean sampling depth remains approximately constant regardless of actual interfiber distance, provided that light with the same arrival time is considered. In practice, taking advantage of this fact is difficult, since it requires measurements of the rare late photons in the presence of an overwhelming amount of early light. This limitation was recently overcome by exploiting an ultrafast time-gated single photon avalanche diode (TG-SPAD) [11], and the application of high-dynamic-range time-of-flight spectroscopy (TOFS) measurements at small (millimeter) source–detector separations in half-space geometries has been demonstrated in connection to functional imaging of brain activation [11] and noncontact diffuse optical imaging [12].

In this Letter, we demonstrate interstitial diffuse optical TOFS based on a single, thin (50 μm core diameter) optical fiber for both light injection and detection. This advancement combines the minimal invasiveness advantage of single needle probes with the larger probe volumes conventionally associated with multiple fiber techniques, thus opening up the field for new applications in interstitial deep tissue probing diffuse optical spectroscopy. By employing high-dynamic-range, time-resolved detection absorption and scattering properties are separable, and we demonstrate that the absorption can be assessed without quantifying the scattering.

Monte Carlo (MC) simulations were employed to investigate the single-fiber approach more closely. Figure 1 illustrates the simulation results of diffusely scattered light reentering a single fiber inserted into an infinite, homogeneously scattering, and nonabsorbing material. Absorption may be added afterward as an exponential decay, $\exp(-\mu_a v t)$ (the Beer–Lambert law), where μ_a is the absorption coefficient and $v = c/n$ is the local speed of light. The parameters for the simulations were: fiber diameter 400 μm and NA $= 0.7$, $n = 1.5$, $g = 0.9$, and $N = 4 \times 10^9$ "photon packets." The total amount of light reentering the fiber was shown to vary with the reduced scattering coefficient, μ_s', of the probed medium as well as the collection efficiency of the fiber, i.e., fiber diameter and NA. Interestingly, temporal shape of the time-dispersion curve was found to be independent of these parameters with two exceptions: first, the amount of very early light (<10 ps) relative to late light depends on the fiber collection efficiency. Changing the NA or reducing the fiber diameter gave no other detectable changes in the shape. Second, changing μ_s' gives a small change in the late part decay of the curve. This may be modeled as an additional exponential decay, $\exp(-\Delta\mu v t)$, where $\Delta\mu$ describes the decay rate due to the change in scattering. Thus, it is not possible to completely distinguish the effects of $\Delta\mu$ and μ_a; absorption properties derived from single-fiber measurements may be subject to a

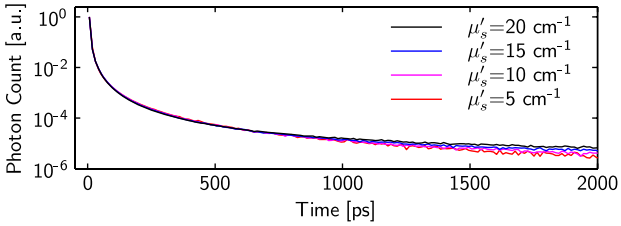

Fig. 1. (Color online) MC simulations of the diffuse reflectance in the single-fiber geometry (nonabsorbing, infinite medium). The curves are normalized against the peak value in order to clarify small difference in the shapes.

small offset, $\Delta\mu$, unless the correct scattering coefficient is known. However, $\Delta\mu$ is, for realistic fiber and scattering properties, small. For example, comparing curves for $\mu_s' = 20$ and 5 cm^{-1} in Fig. 1, the offset is $\Delta\mu = 0.015$ cm^{-1}. This should be compared to realistic absorption coefficients of tissue, e.g., 0.25 cm^{-1} for prostate tissue at 786 nm [5].

From the simulations, it was clear that it is possible to describe the full detected signal (i.e., diffuse and specular reflections) by a semianalytical expression:

$$y_{\mathrm{tot}}(\mu_s', \mu_a, t) = k_d(\mu_s') y_0(t) \exp(-\mu_a v t) + k_s \delta_t, \quad (1)$$

where $k_d(\mu_s')$ is a coefficient, dependent on μ_s' and the fiber collection efficiency, describing the intensity of the diffuse contribution, and $y_0(t)$ is the shape of the diffusively reflected pulse. As shown in Fig. 1, this shape is, to a good approximation, independent of the scattering properties. The term $k_s\delta_t$ models the very early light, dependent on the specular reflection in the fiber end as well as the fiber diameter and NA. δ_t is a Dirac delta and k_s describes the intensity.

Turning to the experimental investigation, the single-fiber approach shares many similarities with recent studies of time-resolved diffuse reflectance at small fiber separations, and this study utilizes similar instrumentation [11]. Briefly, the system is based on time-correlated single photon counting. The source comprises a laser (C450, Fianium Ltd., UK) in combination with an acoustic-optical filter (Neos Technologies, Fla., USA), delivering picosecond pulses at 750 nm. The detector is a custom 100 μm TG-SPAD detector matching the laser repetition rate (40 MHz) while featuring a gate width of 4 ns. By sequentially making measurements at different gate delay times, it was possible to reconstruct TOF curves with a dynamic range of 8 orders of magnitude [13]. The system in [11] was modified for single-fiber operation using a fused fiber splitter (2×2, 50/50) with 50 μm graded index fibers (VISNIR 50/50, OZ Optics, US), as illustrated in the inset of Fig. 2. The source and detector are connected to each of the two fibers in the instrument end of the spliced fiber, while one of the two distal fiber ends was immersed into the tissue phantom to be measured. The other, redundant fiber was immersed into an ink–water suspension, minimizing the specular reflectance and eliminating the diffuse reflectance. The instrument response function (IRF) was recorded with both fiber ends immersed in the ink–water suspension, providing a specular reflection similar to that of the liquid phantoms.

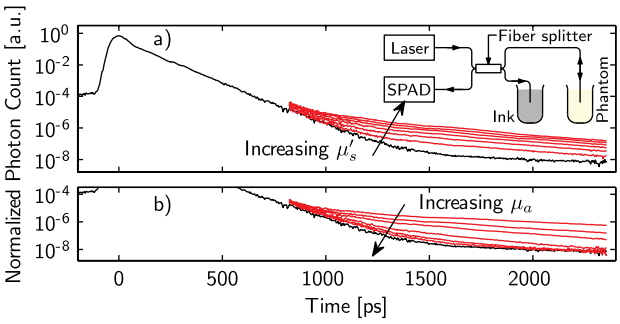

Fig. 2. (Color online) Reconstructed high-dynamic-range TOF curves from (a) the added scattering series (S1) and (b) an added absorption series (A3). In (a), μ_s' is varied from 5.4 to 30.7 cm^{-1}. The slope of the late part is independent of the scattering. In (b), μ_a is varied from 0.03 to 0.23 cm^{-1}. At high absorption, as well as for early times (not shown), the curves closely resemble the IRF (solid black).

Measurements were conducted on tissue simulating phantoms based on calibrated Intralipid (Fresenius Kabi, Germany) and ink (Higgins Ink, Chartpak, Inc., US). All phantom constituents were carefully weighed, allowing the true optical properties of each phantom to be calculated [14,15]. The capability to estimate absorption was studied by conducting added absorber series, where ink was added to the phantom in small increments. Three such series were performed with nominal scattering $\mu_s' \approx 20$ cm^{-1} (A1 and A3) and $\mu_s' \approx 10$ cm^{-1} (A2). The influence of varying scattering properties was investigated using an added scatterer series (S1) with nominal absorption $\mu_a \approx 0.07$ cm^{-1}. In A1 and A2, the full time-of-flight (TOF) curves were recorded. Because of the rapid decay of the reflectance curves (Fig. 1), the early part of the curves is indistinguishable from the IRF. Consequently, in order to reduce the acquisition time in A3 and S1, only the later part of the curves was recorded. This is illustrated in Fig. 2, where data from the series A3 and S1 are shown. The measurements agree with the simulation predictions; in the scattering series, the late curve decay rate is almost independent of the scattering, while the amount of collected diffuse light increases with μ_s'. As expected, the decay rate increases with increasing μ_a in the absorption series. Interestingly, the curves level off to a plateau for later delays. The origin of this behavior is under investigation, but it is not due to detector dark noise. Also, due to imperfections in the curve reconstruction procedure [13], all curves exhibit minor unevenness on a 100 ps timescale.

The model in Eq. (1) was used in the evaluation of all measured data. Here the logarithm of each measured curve was iteratively compared to the logarithm of the convolution of the model and the IRF. The logarithmic scale was required to numerically accommodate the high dynamic range. The function $y_0(t)$ was calculated using a single-fiber MC simulation of 3.6×10^{10} photon packets with the following parameters: $\mu_s' = 20$ cm^{-1}, $\mu_a = 0$, $g = 0.9$, $n = 1.33$, fiber diameter 50 μm, and NA = 0.31. As the system does not measure absolute intensities, the parameters k_d and k_s were set as free parameters in the fitting. Further, only data in the range 822–2200 ps were used in the fitting, where 822 ps represents the first time channel recorded in the case of measurement series A3 and S1.

Figure 3 illustrates the relation between the evaluated and calculated (true) absorption coefficients. For all absorption series, the evaluated μ_a exhibits a linear increase with true absorption, but with a small offset $\sim$0.01 cm^{-1}. This offset is believed to be due to the curve reconstruction procedure or the IRF plateau. For high absorption measurements, $\mu_a \gtrapprox 0.3$ cm^{-1}, the measurement data become increasingly similar to the IRF. Yet, reasonable values for μ_a are recovered. The limitation for $\mu_a \gtrapprox 0.3$ cm^{-1} is not inherent of the single-fiber TOF method and may be alleviated by addressing the plateau

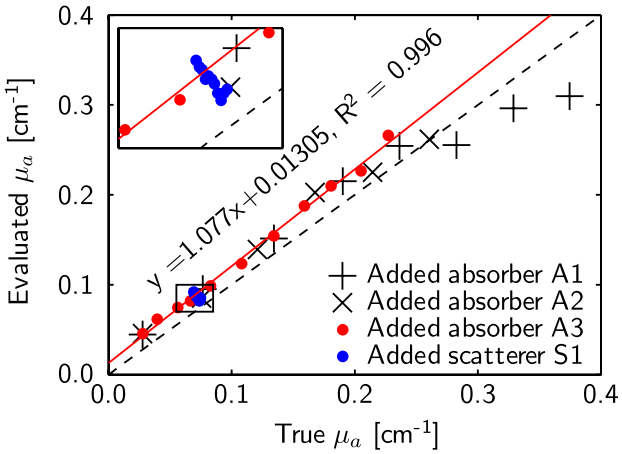

Fig. 3. (Color online) The dashed line shows the expected behavior, and the red solid line shows the best linear fit to the A3 series data. The added scatterer (S1) series is highlighted in the inset. There, the change in true absorption is due to the dilution caused accompanying the addition of more Intralipid.

problem or by increasing the detector/fiber collection efficiency.

Turning to the influence of scattering, no significant differences between A2 ($\mu_s' \approx 10$ cm^{-1}), and A1 or A3 ($\mu_s' \approx 20$ cm^{-1}) were found. As illustrated in the inset of Fig. 3, changing μ_s' from 5.4 to 30.7 cm^{-1} in the scattering series S1, still assuming $\mu_s' \approx 20$ cm^{-1} in evaluation, reveals a change ($\Delta\mu$) in evaluated μ_a of less than 0.01 cm^{-1}, in good agreement with the MC simulation results. From this, it is clear that the small offset observed in the absorption series is not related to the previously discussed scattering-induced offset, $\Delta\mu$.

Regarding the possibilities of also assessing the scattering properties, we note that the influence of μ_s' is primarily limited to the intensity of the diffusively reflected curve, k_d, relative to the specular reflectance, k_s. Thus, careful calibration of the instrumentation may allow model based assessment of μ_s'. However, such assessment is highly sensitive to local inhomogeneities close to the fiber tip, commonly encountered in tissue.

The proposed technique has obvious potential to be improved: an optical fiber with higher NA and a larger core diameter together with a larger area SPAD would increase the sensitivity without influencing the main concept. Also, the SPAD device and gating electronics can possibly be improved for this application by addressing specific bottlenecks and further increasing the dynamic range.

In conclusion, we have demonstrated interstitial TOFS using a single-fiber approach, enabled by time-gated detection. The minimally invasive single-fiber technique is clearly more attractive for many clinical applications, as well as in studies where minimal invasiveness is desired, e.g., in archeological wood or food quality estimation. Further, the approach alleviates the need to keep track of the relative positions of multiple fibers and allows straightforward extraction of the absorption coefficient, which e.g., is directly related to physiological parameters in tissue. Contrary to similar steady-state approaches [1–3,6–8], the "average" absorption in a larger volume is measured, not just what is immediately in front of the fiber. Extraction of the scattering coefficient, providing structural information, may be possible in sufficiently homogeneous materials but would require careful calibration of the equipment.

The authors acknowledge funding from the European Commission Seventh Framework Programme under grant agreements nos. 228334 and 201076, from the Ministero dell'Istruzione dell'Università e della Ricerca of the Republic of Italy, and from the Swedish Research Council under the Executive Programme for Scientific and Technological Cooperation between Italy and Sweden and grant no. 2007-4214.

References

1. M. Johns, C. Giller, D. German, and H. Liu, Opt. Express **13**, 4828 (2005).
2. L. B. Lovat, K. Johnson, G. D. Mackenzie, B. R. Clark, M. R. Novelli, S. Davies, M. O'Donovan, C. Selvasekar, S. M. Thorpe, D. Pickard, R. Fitzgerald, T. Fearn, I. Bigio, and S. G. Bown, Gut **55**, 1078 (2006).
3. J. Antonsson, O. Eriksson, P. Blomstedt, A. T. Bergenheim, M. I. Hariz, J. Richter, P. Zsigmond, and K. Wårdell, J. Neural Eng. **5**, 185 (2008).
4. T. Svensson, S. Andersson-Engels, M. Einarsdóttír, and K. Svanberg, J. Biomed. Opt. **12**, 014022 (2007).
5. T. Svensson, E. Alerstam, M. Einarsdóttír, K. Svanberg, and S. Andersson-Engels, J. Biophoton. **1**, 200 (2008).
6. J. D. Johansson, J. Biomed. Opt. **15**, 057005 (2010).
7. S. C. Kanick, C. van der Leest, J. Aerts, H. Hoogsteden, S. Kascáková, H. J. C. M. Sterenborg, and A. Amelink, J. Biomed. Opt. **15**, 017004 (2010).
8. A. Kim, M. Roy, F. Dadani, and B. C. Wilson, Opt. Express **18**, 5580 (2010).
9. A. Torricelli, A. Pifferi, L. Spinelli, R. Cubeddu, F. Martelli, S. Del Bianco, and G. Zaccanti, Phys. Rev. Lett. **95**, 078101 (2005).
10. L. Spinelli, F. Martelli, S. Del Bianco, A. Pifferi, A. Torricelli, R. Cubeddu, and G. Zaccanti, Phys. Rev. E **74**, 021919 (2006).
11. A. Pifferi, A. Torricelli, L. Spinelli, D. Contini, R. Cubeddu, F. Martelli, G. Zaccanti, A. Tosi, A. Dalla Mora, F. Zappa, and S. Cova, Phys. Rev. Lett. **100**, 138101 (2008).
12. M. Mazurenka, A. Jelzow, B. Ebert, H. Wabnitz, D. Contini, L. Spinelli, A. Pifferi, A. Dalla Mora, A. Tosi, and R. Macdonald, Proc. SPIE **8088**, 80880A (2011).
13. A. Tosi, A. Dalla Mora, F. Zappa, A. Gulinatti, D. Contini, A. Pifferi, L. Spinelli, A. Torricelli, and R. Cubeddu, Opt. Express **19**, 10735 (2011).
14. F. Martelli and G. Zaccanti, Opt. Express **15**, 486 (2007).
15. L. Spinelli, F. Martelli, A. Farina, A. Pifferi, A. Torricelli, R. Cubeddu, and G. Zaccanti, Opt. Express **15**, 6589 (2007).